Updated lattice results for parton distributions

Constantia Alexandrou[a,b], Krzysztof Cichy[c,d], Martha Constantinou[e], Kyriakos Hadjiyiannakou[a], Karl Jansen[f], Fernanda Steffens[f], and Christian Wiese[f]

[a]Department of Physics, University of Cyprus, P.O. Box 20537, 1678 Nicosia, Cyprus
[b]The Cyprus Institute, 20 Kavafi Str., Nicosia 2121, Cyprus
[c]Goethe-Universität Frankfurt am Main, Institut für Theoretische Physik, Max-von-Laue-Strasse 1, 60438 Frankfurt am Main, Germany
[d]Faculty of Physics, Adam Mickiewicz University, Umultowska 85, 61-614 Poznań, Poland
[e]Temple University, 1925 N. 12th Street, Philadelphia, PA 19122, USA
[f]John von Neumann Institute for Computing (NIC), DESY, Platanenallee 6, 15738 Zeuthen, Germany

July 11, 2017

Abstract

We provide an analysis of the x-dependence of the bare unpolarized, helicity and transversity iso-vector parton distribution functions (PDFs) from lattice calculations employing (maximally) twisted mass fermions. The x-dependence of the calculated PDFs resembles the one of the phenomenological parameterizations, a feature that makes this approach very promising. Furthermore, we apply momentum smearing for the relevant matrix elements to compute the lattice PDFs and find a large improvement factor when compared to conventional Gaussian smearing. This allows us to extend the lattice computation of the distributions to higher values of the nucleon momentum,which is essential for the prospects of a reliable extraction of the PDFs in the future.

1 Introduction

Finding a way to a computation of parton distribution functions (PDFs) with lattice QCD techniques has been a long standing goal in lattice gauge theory. The basic problem roots in the Euclidean nature of lattice QCD that does not allow for a direct calculation of the PDFs, which are usually defined as light cone correlations in the rest frame of the target. Therefore, lattice QCD computations have focused on moments of PDFs, form factors and related quantities. The calculations have been very successful with important results connecting to phenomenology and experiment, see [1, 2, 3, 4, 5] for recent reviews and [6] for an overview of lattice activities on hadron structure.

Moreover, lattice QCD calculations concerned with hadron structure are now being performed at or close to the physical value of the pion mass [7, 8, 9, 10, 11, 12, 13, 14] allowing for a significantly improved control of the involved systematic uncertainties,

since the previously required chiral extrapolation to the physical value of the quark mass can be avoided. In addition, in recent works also the disconnected diagrams – which were often neglected in the past – have been taken into account, involving a very high statistics of $\mathcal{O}(10^5)$ measurements [15, 16, 17, 18].

Despite this success, a direct calculation of PDFs remains highly desirable for several reasons. First, having the non-perturbative functional shape of the PDFs over a broad range of the momentum fraction (Bjorken variable) x available would provide essential information on the structure of hadrons, as predicted solely by QCD. Furthermore, the knowledge of the PDFs would allow for a direct comparison to experimental results and phenomenological analyses of deep inelastic scattering data. In particular, the flavor structure of the nucleon sea is highly nontrivial, and the observed asymmetry between the up and down antiquark distributions (see [19] for a review) is an intrinsically non-perturbative QCD effect [20, 21]. However, the lattice calculations have been restricted to the first two or three moments of PDFs, and thus providing only limited insight into the structure of hadrons.

A possible way towards a direct calculation of PDFs has been proposed in Ref. [22]. The idea is to compute the so-called quasi distributions where the Wilson line connecting the quarks in the nucleon is taken in the spatial directions, avoiding thus the difficulty of the light cone dominance. The quasi distributions can be related to the PDFs through a suitable matching procedure. In the language of an effective field theory, it means that parton distributions can be extracted from the lattice observables using a systematic expansion in the inverse powers of the nucleon momentum [23]. The approach of Ref. [22] has already been tested for the bare distribution functions in [24, 25, 26, 27] and it could be demonstrated that at least on a qualitative level, the shape of the physical distribution functions is reproduced. A most remarkable finding of these lattice calculations has been that the quark-antiquark asymmetry in the PDFs does come out automatically from the first principles lattice QCD calculations without any additional input.

In this paper, we extend the computation of PDFs on the lattice, compared to our previous lattice study [26], in several ways: in addition to the unpolarized PDFs, we now also include the helicity and the transversity PDFs. Also, all results presented in this paper (using the standard Gaussian smearing of quark fields) have a substantially increased statistics of about 30000 measurements, which is about a factor of 6 improvement compared to [26]. This allows us to go to larger momenta and thus a much better control of the matching to the physical distribution can be achieved. We also provide a test of the recent new matching formula of Ref. [28]. As a new, more technical step, we have implemented a recently developed type of smearing of quark fields, the momentum smearing [29], and we find a significant improvement of the signal-to-noise ratio when compared to the previous momentum independent (Gaussian) smearing. Finally, for illustration purposes, we demonstrate how the method of quasi distributions works in practice, by performing the necessary steps of this procedure at tree-level of perturbation theory, i.e. for free quarks and show how the expected δ-function distribution is approached.

The still open question, which however goes much beyond the scope of this paper, is the renormalization of the matrix elements needed to compute the quasi distributions.

Although there are already first works towards the renormalization of PDFs [30, 31, 28], a full, in particular non-perturbative analysis, including a subtraction of power-like divergences combined with non-perturbative lattice calculations is still missing. However, work in this direction is in progress by us and will be discussed in the near future in a separate work[1].

The paper is organized as follows. In Section 2, we provide the theoretical principles and the setup to compute the quasi distributions on the lattice. In Section 3, numerical results are presented, including the matching to physical quark distributions. We finally conclude and discuss the prospects of this approach in Section 4.

2 Theoretical principles and lattice techniques

2.1 Quasi-parton distributions and matching to physical parton distributions

Parton distributions can be defined either in the infinite momentum frame (IMF), according to Feynman's original proposal [34], or in the rest frame of the nucleon, this last one being the definition usually found in the literature. In the original definition, because the nucleon is with infinite momentum, there is no time for the partons to interact and thus they are essentially free. On the other hand, in the nucleon rest frame, the distributions are given by light cone correlations

$$q(x,\mu) = \int_{-\infty}^{+\infty} \frac{d\xi^-}{4\pi} e^{-ixP^+\xi^-} \langle P|\overline{\psi}(\xi^-)\gamma^+ W(\xi^-,0)\psi(0)|P\rangle, \tag{1}$$

where γ^+ is the Dirac structure in the unpolarized case, μ is the renormalization scale, $\xi^- = (\xi^0 - \xi^3)/\sqrt{2}$, $P^+ = (P^0 + P^3)/\sqrt{2} = M/\sqrt{2}$, and $W(\xi^-,0) = e^{-ig\int_0^{\xi^-} d\eta^- A^+(\eta^-)}$ is the Wilson line connecting the point 0 to the point ξ^-. This definition is completely equivalent to that of the IMF [35] meaning that, in principle, one could calculate the distributions using any of the two approaches. In practice, however, if we use lattice QCD, we simply cannot have infinite momentum because the maximum momentum that can be reached on the lattice is limited by the finite lattice spacing a. We are thus left with Eq. (1), which, in turn, cannot be calculated on the lattice, because it is light cone dominated, $\xi^2 = t^2 - \vec{r}^2 \sim 0$, i.e. we have access to a single point only in Euclidean space. Nevertheless, we can calculate the quasi distributions, which are defined (in the unpolarized case) as

$$\tilde{q}(x,P_3) = \int_{-\infty}^{\infty} \frac{dz}{4\pi} e^{-izk_3} \langle P|\bar{\psi}(0,z)\gamma^3 W(z)\psi(0,0)|P\rangle + \mathcal{O}\left(\frac{\Lambda_{QCD}^2}{P_3^2}, \frac{M^2}{P_3^2}\right), \tag{2}$$

where $P = (M,0,0,P_3)$, $k_3 = xP_3$ is the quark momentum in the z-direction, and $W(z) = e^{-ig\int_0^z dz' A_3(z')}$. Because of the finite momentum, some quarks can carry more

[1] After the submission of this manuscript we have indeed developed a full renormalization prescription [32, 33].

momentum than the nucleon itself or even move backwards, and because of this one can have $x > 1$ or $x < 0$, and the usual partonic interpretation is lost. Also, there are higher twist (HT) and target mass corrections (TMCs) that need to be applied. In particular, the TMCs are essential to bring the quasi distributions to their correct support in x [26].

The quasi distributions represent the would-be distributions of a nucleon moving in one particular direction, the third direction as defined in Eq. (2), with a large but finite momentum. Because the infrared physics is the same for a nucleon with infinite momentum and a nucleon moving with a finite (and large) momentum, the difference between the quark distributions and the quark quasi distributions should be in the ultraviolet region (UV) only, and thus can be perturbatively calculated [36, 26],

$$\begin{aligned} q(x,\mu) &= \tilde{q}(x,\Lambda,P_3) - \frac{\alpha_s}{2\pi}\tilde{q}(x,\Lambda,P_3)\delta Z^{(1)}\left(\frac{\mu}{P_3},\frac{\Lambda}{P_3}\right) \\ &\quad -\frac{\alpha_s}{2\pi}\int_{-x_c}^{-|x|/x_c} Z^{(1)}\left(\xi,\frac{\mu}{P_3},\frac{\Lambda}{P_3}\right)\tilde{q}\left(\frac{x}{\xi},\Lambda,P_3\right)\frac{d\xi}{|\xi|} \\ &\quad -\frac{\alpha_s}{2\pi}\int_{+|x|/x_c}^{+x_c} Z^{(1)}\left(\xi,\frac{\mu}{P_3},\frac{\Lambda}{P_3}\right)\tilde{q}\left(\frac{x}{\xi},\Lambda,P_3\right)\frac{d\xi}{|\xi|} + \mathcal{O}(\alpha_s^2). \end{aligned} \tag{3}$$

Here, Λ is the UV cutoff and $x_c \sim \Lambda/P_3$ is the maximum x value for a nonzero $\tilde{q}(x,\Lambda,P_3)$. For the wave function, $\delta Z^{(1)}$, and the vertex, $Z^{(1)}$, corrections, we employ the recent results of [28]. In this work, the linearly divergent terms in Λ/P_3, present in $\delta Z^{(1)}$ and in $Z^{(1)}$, are removed through the addition of a mass counterterm, implying that the only divergence remaining in the matching is logarithmic (see, for instance, Eq. (A9) of [26]). The linear divergence appearing in the lattice calculation of $\tilde{q}\,(x,\Lambda,P_3)$, however, remains. More on this point can be found in Section 2.2.

In the end, we want the momentum to be as large as possible, so that any correction dependent on the finite value of P_3 is sufficiently small, and the matching between the quasi distributions and the distributions, encapsulated by Eq. (3), is valid. In the next subsection, we will discuss how this can be achieved on the lattice.

In this work, we calculate matrix elements of operators with the Dirac structure in Eq. (2):

- γ_3, for the case of the unpolarized quasi distributions $\tilde{q}(x,\Lambda,P_3)$,
- $\gamma_3\gamma_5$, for the case of the helicity quasi distributions $\Delta\tilde{q}(x,\Lambda,P_3)$,
- $\gamma_3\gamma_j$ $(j=1,2)$, for the case of the transversity quasi distributions $\delta\tilde{q}(x,\Lambda,P_3)$.

2.2 Matrix elements

The relation between the quasi distributions and the matrix elements for the unpolarized case is

$$\langle P|\bar{\psi}(0,z)\gamma_3 W(z)\psi(0,0)|P\rangle = \overline{u}(P)h(P_3,z)u(P)\,, \tag{4}$$

with

$$\tilde{q}(x,\Lambda,P_3) = 2P_3 \int_{-\frac{L}{2}}^{+\frac{L}{2}} \frac{dz}{4\pi} e^{-ixP_3 z} h(P_3,z)\,, \tag{5}$$

where $\Lambda = 1/a$, a is the lattice spacing and L is the spatial extent of the lattice. For the helicity and transversity quasi distributions, one only replaces γ_3 by the desired Dirac structure.

The required matrix elements are obtained from the ratio of suitable two- and three-point functions. The three-point function is constructed in the usual way with boosted nucleon interpolating fields and a local operator,

$$C^{3pt}(t,\tau,0;\vec{P}) = \left\langle N_\alpha(\vec{P},t)\mathcal{O}(\tau)\overline{N}_\alpha(\vec{P},0)\right\rangle, \tag{6}$$

where $\langle ...\rangle$ is the average over a sufficiently large number of gauge field configurations. The boosted nucleon field is defined via the Fourier transformation of quark fields in position space,

$$N_\alpha(\vec{P},t) = \Gamma_{\alpha\beta}\sum_{\vec{x}} e^{-i\vec{P}\vec{x}}\epsilon^{abc}u^a_\beta(x)\left(d^{b^T}(x)\mathcal{C}\gamma_5 u^c(x)\right), \tag{7}$$

where $\mathcal{C}$ is the charge conjugation matrix, chosen to be $i\gamma_0\gamma_2$, and $\Gamma_{\alpha\beta}$ is the parity projector, depending on the Dirac structure used. We use here the parity plus projector $\Gamma = \frac{1+\gamma_4}{2}$ for the case of γ_3, $\Gamma = i\gamma_3\gamma_5\frac{1+\gamma_4}{2}$ for the case of $\gamma_3\gamma_5$, and $\Gamma = i\gamma_k\frac{1+\gamma_4}{2}$ (with $k \neq j \neq 3$) for the case of $\gamma_3\gamma_j$. The operator at vanishing momentum transfer ($Q^2 = 0$) to be inserted in Eq. (6) is obtained by choosing

$$\mathcal{O}(z,\tau,Q^2=0) = \sum_{\vec{y}} \overline{\psi}(y+\hat{e}_3 z)\gamma_3 W_3(y+\hat{e}_3 z,y)\psi(y), \tag{8}$$

for the case of γ_3, where $y = (\vec{y},\tau)$. Similar expressions hold for the cases of $\gamma_3\gamma_5$ and $\gamma_3\gamma_j$. The Wilson line is computed as a product of gauge links along the chosen axis, where only the shortest path is considered

$$W_j(y+z\hat{e}_j,y) = U_j(y+(z-1)\hat{e}_j)\ldots U_j(y+\hat{e}_j)U_j(y). \tag{9}$$

Due to the rotational invariance on the lattice, we are certainly not restricted to the 3 direction and can easily generalize the above expressions to the other two directions.

To complete the calculation, we also need the two-point function, which is also constructed from the nucleon interpolating field as in Eq. (6), but without the insertion of the operator. With this in mind, the desired matrix element for the case of γ_3 is extracted from

$$\frac{C^{3pt}(t,\tau,0;\vec{P})}{C^{2pt}(t,0;\vec{P})} \overset{0\ll\tau\ll t}{=} \frac{-iP_3}{E}h(P_3,\Delta z), \tag{10}$$

with $E = \sqrt{(P_3)^2+M^2}$ the total energy of the nucleon. For the helicity, $\Delta h(P_3,\Delta z)$, and the transversity, $\delta h(P_3,\Delta z)$, matrix elements, the pre-factor $\frac{-iP_3}{E}$ is absent, which can be easily verified from their definition from Eq. (4).

Due to the symmetric structure of the operator, there is a relation between the negative and positive z direction of the matrix elements. To see this, one can apply the gauge link identity $U_{-j}(x) = U_j(x - \hat{e}_j)^\dagger$ to Eq. (9), which results in $W_j(y + z\hat{e}_j, y) = W_j(y, y + z\hat{e}_j)^\dagger$. Thus, one obtains the relation $\mathcal{O}(z, \tau) = -\mathcal{O}(-z, \tau)^\dagger$ for the Euclidean operator defined in Eq. (8), due to its translational invariance structure. For the cases of $\gamma_3\gamma_5$ and $\gamma_3\gamma_j$, however, one has $\mathcal{O}(z, \tau) = +\mathcal{O}(-z, \tau)^\dagger$. Taking into account the pre-factors of Eq. (10), one then obtains

$$\begin{aligned} h(P_3, z) &= h(P_3, -z)^\dagger, \\ \Delta h(P_3, z) &= \Delta h(P_3, -z)^\dagger, \\ \delta h(P_3, z) &= \delta h(P_3, -z)^\dagger. \end{aligned} \tag{11}$$

These are completely general equations that not only can be used as a cross-check to our lattice results, but also have the fundamental consequence of producing an asymmetry between the quark and antiquark distributions, as it will be clear in Section 3.3. For the operators themselves, we will compute only the iso-vector quark combination, i.e. a τ^3 matrix in flavor space is inserted, as this avoids possible operator mixing and disconnected contributions. Consequently, the resulting matrix elements will carry a $u - d$ superscript.

2.3 Smearing of quark fields

Usually the signal-to-noise ratio for a boosted nucleon is not strong, and to enhance it one introduces Gaussian smearing (S) in the quark fields [37, 38]. The results presented in [26, 39] use such smearing and one sees that the errors increase rapidly with the injected momentum, making this approach unfeasible for $P_3 > 6\pi/L$. This upper limit imposes a serious constraint on the simulations, because we want to reach values for the momentum where higher order corrections in α_s to Eq. (3) can be safely neglected. Also, we want the corrections from the matching itself, as well as the ones from TMCs and from HTs, to be small. In other words, it is desirable to have a nucleon with momentum that, in practice, is large enough such that the lattice data start to show saturation, in the sense that the computed quasi distributions are essentially unchanged as the momentum grows.

In Ref. [29], a new type of smearing, called momentum smearing (S_{mom}), was proposed where the quark fields are modified as

$$S_{mom}\psi(x) = \frac{1}{1 + 6\alpha}(\psi(x) + \alpha \sum_j U_j(x) e^{ik\hat{e}_j} \psi(x + \hat{e}_j)), \tag{12}$$

where $k = \zeta P$, with P the lattice momentum of the nucleon and ζ a tunable parameter, α is a positive constant, and $U_j(x)$ are the gauge links in the direction j. Throughout this work, we use 50 steps of smearing with $\alpha = 4$. As for ζ, we use 0.45, which is the value found to be optimal in [29]. The usual Gaussian smearing $S\psi(x)$ corresponds to dropping the exponential factor in (12). The immediate consequence of the exponential

factor is that, when going to momentum space, the smearing of the field is not around 0, but around the shifted momentum k. This has the enormous advantage that we can tune the smearing to be done for higher values of the nucleon momentum, and not only to values close to zero, as with the standard Gaussian smearing, implying that the quark field smearing may now be effective for large values of the boosted nucleon momentum. In the next section, we explore this possibility numerically.

When computing the three-point functions using Gaussian smearing, we have some freedom on how to treat the quark propagator connecting the sink position with the point where the operator is inserted. In principle, there are two different ways of computing this all-to-all propagator. The first one is to use the sequential method [40]. The shortcoming of this method is that the sink position and the nucleon momentum at the sink have to be fixed, making this approach not optimal if we want to compute the matrix elements at several values of the nucleon momentum.

The second method is the stochastic method [41] that uses stochastic Z^4 noise sources on a single time slice for the computation of the all-to-all propagator. This method is very flexible when using different momenta and projectors, however it adds stochastic noise to the calculation.

In our previous work [26, 42], we tested both methods and found that at the expense of the same computation effort, they were compatible. Nonetheless, the stochastic method is more flexible when computing several values of the boosted nucleon momentum, thus our initial choice was to use stochastic sources, even if this introduces more noise to the system.

However, due to the recent introduction of momentum smearing (cf. Eq. (12)), the premises that led to the choice of the stochastic method are not satisfied anymore. When using momentum smearing, one reduces the noise for larger momenta dramatically, with the drawback of having to perform separate inversions for each momentum. Thus, the flexibility of the stochastic method is lost and it is preferable to use the sequential method. In this way, in the present work, we use the stochastic method for the standard Gaussian smearing and the sequential method when using the new momentum smearing.

2.4 HYP smearing

As in our earlier study, we apply HYP smearing [43] to the gauge links in the inserted operator. This is a lattice technique used to smoothen the gauge links, and such procedure is expected to bring the renormalization factors closer to the corresponding tree-level values.

This is particularly useful for the present status of our work, because we still have not computed the operator renormalization, while the renormalization factors for the local bilinear quark operators are known: $Z_V = 0.625(2)$, $Z_A = 0.7556(5)$, and $Z_T = 0.7483(6)$ in the $\overline{\text{MS}}$ scheme, at $\mu = 2$ GeV, where we used the renormalization functions from Ref. [44], which have also been employed for other nucleon structure quantities [7, 45].

In this way, in order to estimate how operator renormalization could affect the present results, we apply 5 steps of HYP smearing, which, according to our previous study, is close to saturating the effects of the smearing. In fact, it is shown in Ref. [31] that the

linear divergences have their origin in the tadpole-type diagrams and that HYP smearing of the Wilson line has, practically, the effect of removing such linear divergences.

2.5 Lattice setup

Ensemble. We use a $32^3 \times 64$ ensemble from an ETMC (European Twisted Mass Collaboration) production ensemble [46], with $N_f = 2 + 1 + 1$ flavors of maximally twisted mass fermions. The bare coupling is $\beta = 1.95$, corresponding to a lattice spacing of $a \approx 0.082\,\text{fm}$ [47], while the twisted mass parameter is $a\mu = 0.0055$, which gives a pion mass of $m_{PS} \approx 370\,\text{MeV}$.
Statistics. For the computation of matrix elements, we first extend our previous calculation using Gaussian smearing. To that end, we now employ 1000 gauge configurations, each with 15 point source forward propagators and 2 stochastic propagators, resulting in total 30000 measurements, which is about 6 times more than our previous paper [26]. For our exploratory computation using the momentum smearing method, we use 50 gauge configurations for momentum $6\pi/L$ and $8\pi/L$, and 100 gauge configurations for momentum $10\pi/L$. In both cases, we use 3 sequential quark propagators, one for each spatial direction, resulting in a total of 150 measurements for $P_3 = 6\pi/L$ and $8\pi/L$, and 300 measurements for $P_3 = 10\pi/L$. As we will demonstrate below, even with this rather small statistics, we obtain good results thanks to the new momentum smearing.

3 Numerical results

In this section, we show our numerical results. For purely illustrative purposes, we start with a simple free theory demonstration that indeed the expected quark distribution, the Dirac delta function at $x = 1/3$, is approached when sufficiently increasing the nucleon momentum. Then, we discuss the results for the matrix elements needed for the computation of quasi distributions. In particular, we show the tremendous improvement from using the recently introduced momentum smearing. Next, we move on to the quasi distributions and the physical parton distribution functions obtained from the matching procedure. We also discuss the importance of HYP smearing and finally, we show results for the moments of the distributions determined in this work.

3.1 Free quark distributions

Free quark distributions are obtained from the definitions (1) or (2) when one sets the gauge links equal to 1. With unity gauge links, the limitation connected to a poor signal-to-noise ratio disappears, as well as the problem of renormalization, and, given this, the free quark distributions are the perfect prototype to make explicit the fundamental point of the present approach: the purely spatial correlations calculated in the lattice, the quasi-distributions, tend to what we expect for the quark distributions as $P_3 \to \infty$. If the quasi-distribution approach is, thus, to be valid, the resulting distributions should tend to a Dirac delta function, centered in $x = 1/3$, as P_3 increases. We show

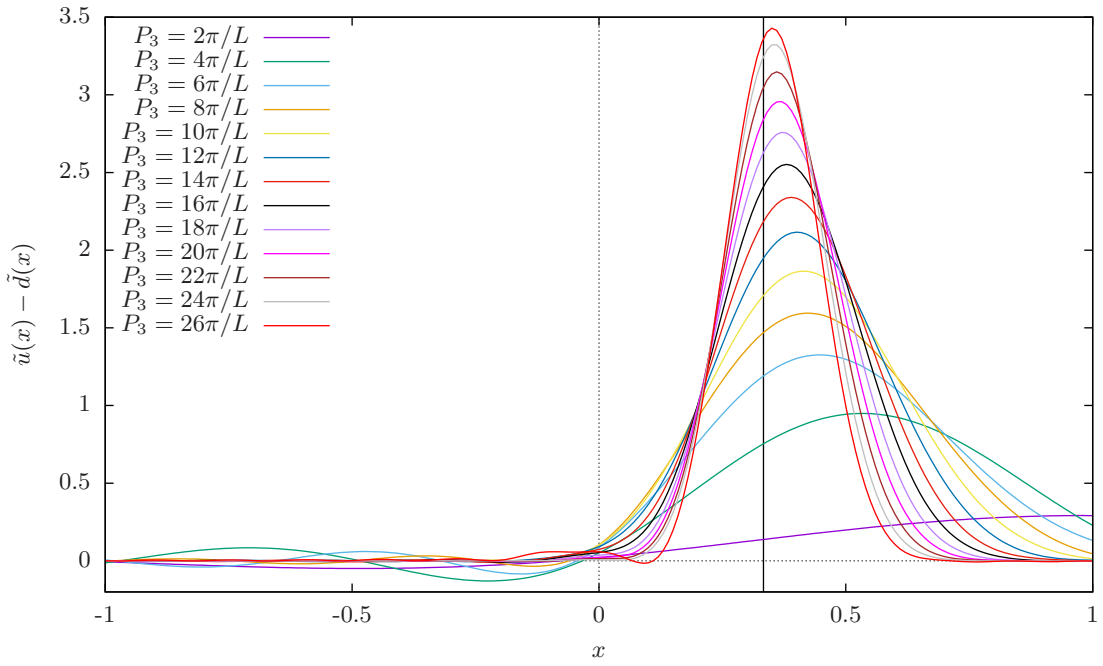

Figure 1: Free quark distributions for a lattice of size $48^3 \times 96$. As expected, the distributions tend to a Dirac delta at $x = 1/3$ as the nucleon momentum grows.

in Fig. 1 our results for a lattice of size $48^3 \times 96$, for a nucleon with momentum from $P_3 = 2\pi/L$ to $P_3 = 26\pi/L$. The computations are done with a source-sink separation of 12. The resulting distributions are a very pedagogical illustration on the foundations of the method for calculating quark distributions discussed in this work. It shows clearly that as the nucleon momentum increases, the probability of having quarks carrying a negative fraction of the nucleon momentum, or also carrying more momentum than the whole nucleon itself, is suppressed to zero. Simultaneously, the shape of the distributions changes to what is physically expected, namely for large P_3 they start to become sharply distributed around 1/3. The Dirac delta function should be recovered in the combined continuum and infinite source-sink separation limits. This is, however, beyond the scope of the present work.

The results shown in Fig. 1 for the case of free quarks are a fair indication that one should push the calculation of the quasi distributions to values of the nucleon momentum as high as computationally possible in the lattice.

3.2 Matrix elements

In Figs. 2 and 3, we show the matrix elements for the unpolarized $h^{u-d}(P_3, z)$ and the helicity $\Delta h^{u-d}(P_3, z)$ cases, calculated for the 3 lowest lattice momenta, $P_3 = 2\pi/L, 4\pi/L$, and $6\pi/L$, with Gaussian smearing and high statistics (see Sec. 2.5). For the configurations used here, these correspond, in physical units, to $P_3 = 0.49$, 0.98 and 1.47 GeV, respectively. Compared to our previous result, the errors are smaller by a factor of about

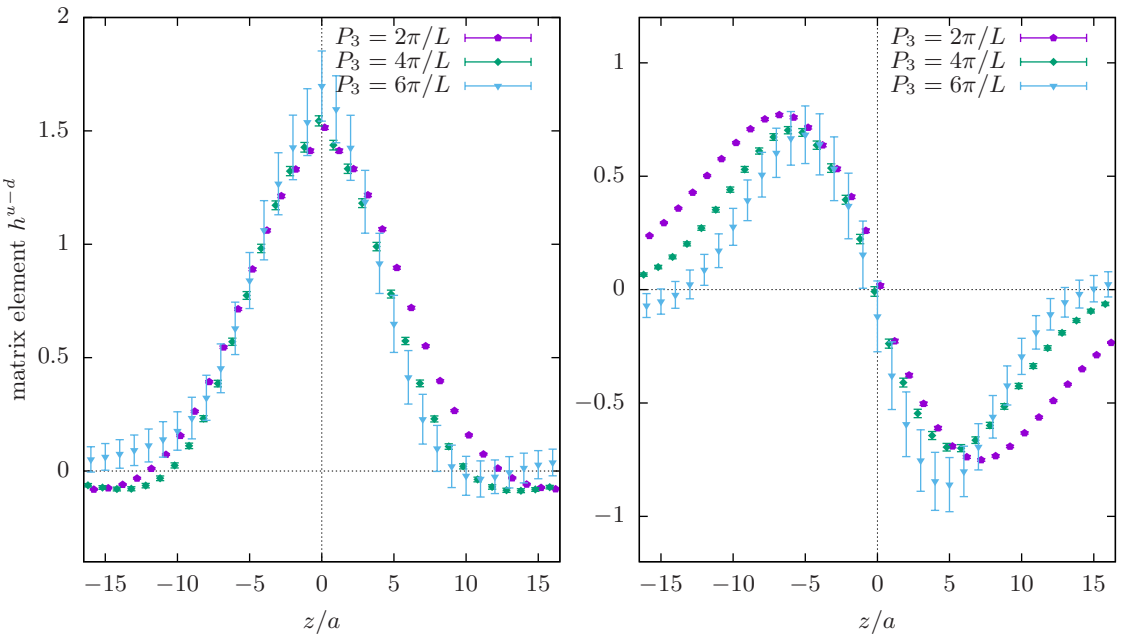

Figure 2: Real (left) and imaginary (right) parts of the matrix elements for the case of the vector operator.

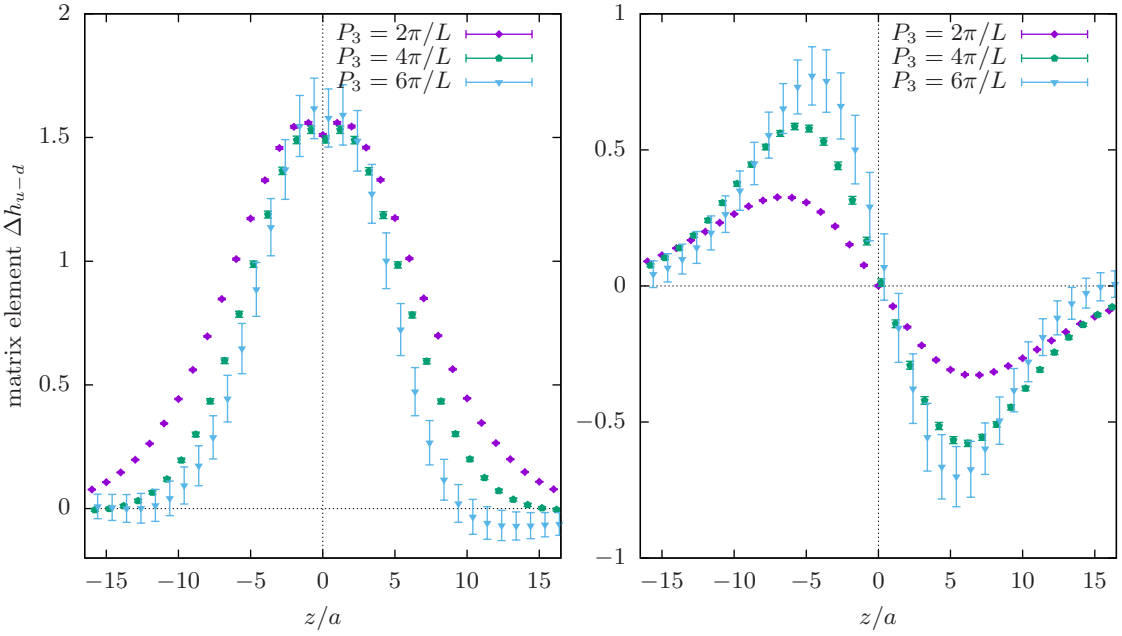

Figure 3: Real (left) and imaginary (right) parts of the matrix elements for the case of the axial-vector operator.

2.5, making them very precise for the two lowest momenta, but still somewhat big for $P_3 = 6\pi/L$, which imposes, as discussed in the beginning of this section, a serious limitation. We note that for lower momenta, $P_3 = 2\pi/L$ and $4\pi/L$, the matrix elements for the unpolarized case are not compatible with zero for the largest computed Wilson lines lengths $|z/a| = 16$. This affects the normalization of the extracted PDFs, and indicates large corrections connected to the finite value of P_3, presumably too large to make already contact to the physical PDFs with these momenta, as clearly seen in the plots of the left side of Fig. 5 of Ref. [26]. Thus, these momenta are too low to be taken into account in the extraction of PDFs, e.g. in the extrapolation to infinite momentum that will be part of the procedure when we aim at calculations to be compared to the phenomenological results (which we plan for the physical pion mass ensembles of ETMC and after addressing a suitable renormalization, see Sec. 4). For this reason, a check of the normalization of the resulting PDFs, which is done in Sec. 3.5, is very important.

To overcome the restriction on the values of the nucleon momentum that can be used, we now employ the momentum smearing on the quark fields, Eq. (12), and recalculate the matrix elements $h^{u-d}(P_3, z)$ and $\Delta h^{u-d}(P_3, z)$. In practice, we use a Gaussian smearing routine and include gauge links with a complex phase $e^{ik\hat{j}}$. For now, we follow [29] and choose ζ to be 0.45.

In addition, we also calculate the matrix elements of the transversity operator, $\delta h^{u-d}(P_3, z)$. The computation is done for momentum $P_3 = 6\pi/L$, $8\pi/L$ and $10\pi/L$ for the case of $h^{u-d}(P_3, z)$, and for $P_3 = 6\pi/L$ for the cases of $\Delta h^{u-d}(P_3, z)$ and $\delta h^{u-d}(P_3, z)$.

We first compare the $h^{u-d}(P_3, z)$ matrix elements using the two different approaches for the smearing of the quark fields, for the case of $P_3 = 6\pi/L$ only. The result is shown in Fig. 4 (in this case, we have symmetrized (antisymmetrized) the real (imaginary) parts of the matrix elements). The two different methods for the smearing give compatible results for the matrix elements, and it is remarkable that the number of measurements necessary for the momentum smearing to match the results from the Gaussian smearing is smaller by a factor of 200. The compatibility of the results from both smearings also suggests that the contamination by excited states is, in the analyzed matrix elements, very similar, i.e. it is very small at $P_3 = 6\pi/L$, as we have explicitly shown in our previous investigation [26] by comparing two different source-sink separations. However, excited states contamination is expected to increase at higher P_3 [48]. Hence, this systematic effect will be thoroughly investigated in future work aimed at extracting PDFs directly at the physical pion mass.

We also show the continuum dispersion relation for the nucleon, using momenta $P_3 = 4\pi/L, 6\pi/L, 8\pi/L, 10\pi/L$ (all from momentum smearing). We find that the relativistic relation between the energy and the momentum $p \equiv P_3$, $E^2 = m^2c^4 + p^2c^2$ is satisfied, i.e. the fit of this relation to our lattice data describes the data very well and the fitted value of the speed of light is $c = 1.023(40)$, i.e. it is compatible with the expected value of $c = 1$ in our units. The nucleon mass in lattice units extracted from this fit, $amc^2 = 0.517(22)$, is also compatible with its direct extraction for a nucleon at rest, $amc^2 = 0.503(2)$ (with $c = 1$) [45].

Having established the importance of momentum smearing for the quark fields, we

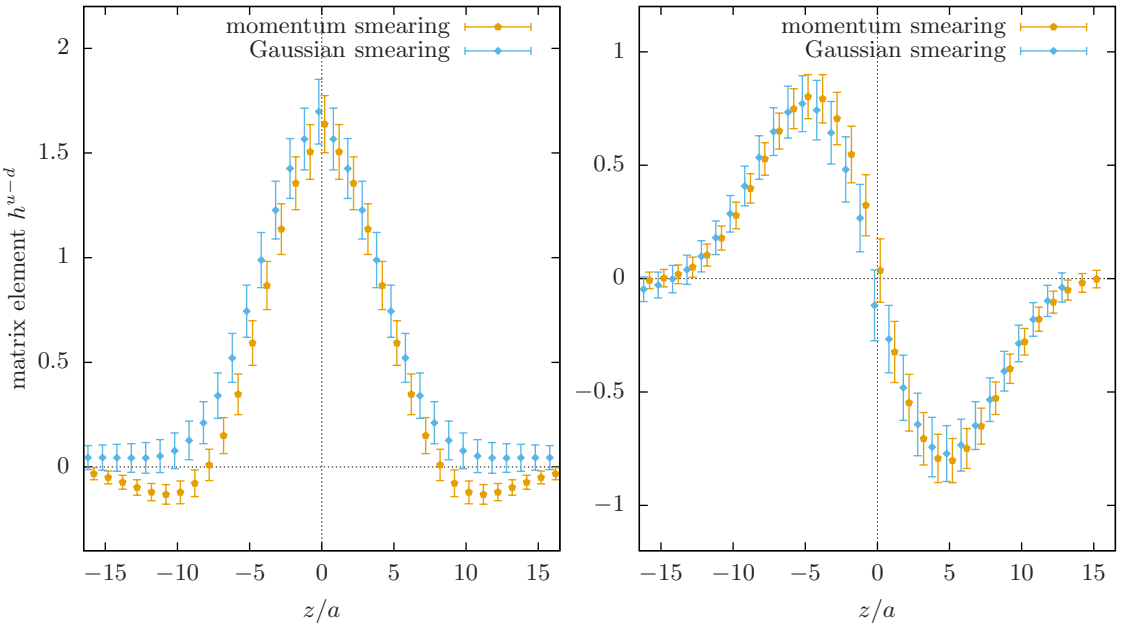

Figure 4: Comparison of two different methods for the smearing of the quark fields for the computation of the matrix element $h^{u-d}(P_3, z)$. One is the standard Gaussian smearing, where 30000 measurements were used. The other is the new momentum smearing, where similar results to those of Gaussian smearing are achieved using only 150 measurements, for the case of momentum $P_3 = 6\pi/L$. In this plot, the real (imaginary) parts of the matrix elements were symmetrized (antisymmetrized).

show in Fig. 6 the matrix elements $h^{u-d}(P_3, z)$ for $P_3 = 6\pi/L$, $8\pi/L$ and $10\pi/L$. With this, we are now ready to calculate the quasi distributions using Eq. (5), and the corresponding quark distributions through Eq. (3) after applying the TMCs. This is done in the next subsection.

In Fig. 7, we show results for the matrix elements of helicity $\Delta h^{u-d}(P_3, z)$ and, for the first time in our work, the transversity distribution $\delta h^{u-d}(P_3, z)$ for $P_3 = 6\pi/L$ and the usage of momentum smearing.

3.3 Quark distributions

In this section, we compute the iso-vector quark quasi distributions and the iso-vector quark distributions in the nucleon, using the matrix elements calculated in the previous subsection, together with Eqs. (3) and (5). We also apply the TMCs (for all employed Dirac structures, corresponding to the unpolarized, helicity and transversity cases) using for them the prescription of [26],

$$\tilde{q}(x, P_z) = \tilde{q}^{(0)}(\xi, P_z)/(1 + \nu\xi^2), \tag{13}$$

where $\xi = 2x/(1 + \sqrt{1 + 4\nu x^2})$ is the Nachtmann variable, $\nu = M_N^2/4(P_3)^2$ (M_N – nucleon mass), and the superscript (0) means that the TMCs have been taken into

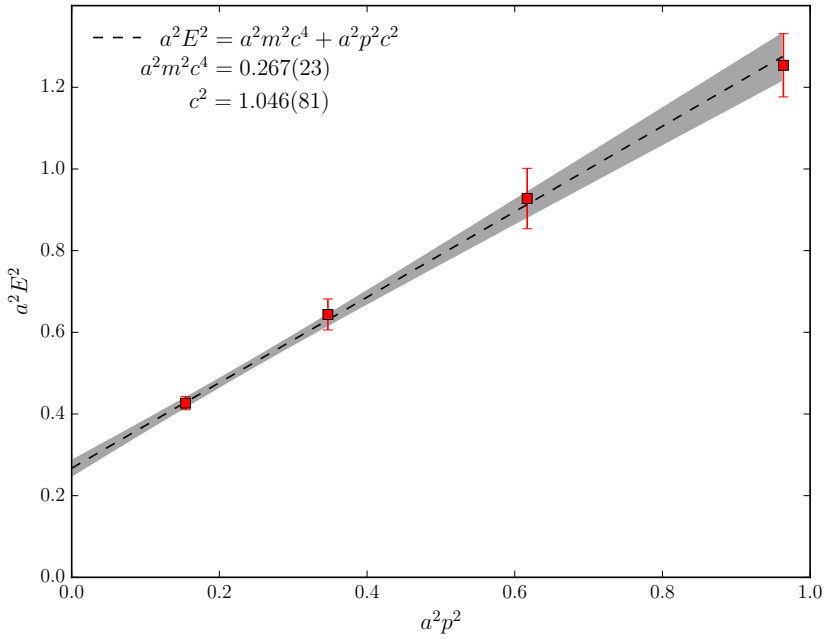

Figure 5: Energy of the nucleon as a function of the momentum boost $p \equiv P_3$. We fit the relativistic relation between the energy and the momentum, $E^2 = m^2c^4 + p^2c^2$ and find the speed of light $c^2 = 1.046(81)$ and the (squared) nucleon mass in lattice units $a^2m^2c^4 = 0.267(23)$.

account. In Ref. [25], an improved prescription for TMCs, which avoids the problem of non-preservation of the norm of the distributions, was presented. However, as shown in Fig. 8, for the values of the nucleon momentum that are the main interest of this work ($P_3 \geq 6\pi/L$) there is, in practice, no difference between the two prescriptions, mostly in the intermediate and large x regions, which are the regions where the quasi distributions approach is applicable. For $P_3 = 8\pi/L$, the difference between the two prescriptions is essentially non existing for the whole x region. We also do not apply the corrections in Λ_{QCD}/P_3, because of the large values of P_3 used in this work to compute the quasi distributions.

For the UV cutoff, we use $\Lambda = 1/a \approx 2.5$ GeV, this being also our choice for the renormalization scale μ where the distributions are defined. For the bare coupling, we use $\alpha_s = 6/(4\pi\beta)$, which, for the lattice setup employed here, corresponds to $\alpha_s \approx 0.245$. Of course, in the future, a full renormalization program will have to be carried out, implying the independence of the final results on Λ. In this same line, we also notice that the integrals in Eq. (3) are cutoff dependent through their dependence on $x_c \sim \Lambda/P_3$. This cut in x, x_c, marks the region in x where $\tilde{q}(x > x_c, \Lambda, P_3) = 0$. Of course, $x_c \geq 1$ by construction, since the nucleon boost can not be larger than the UV cutoff.

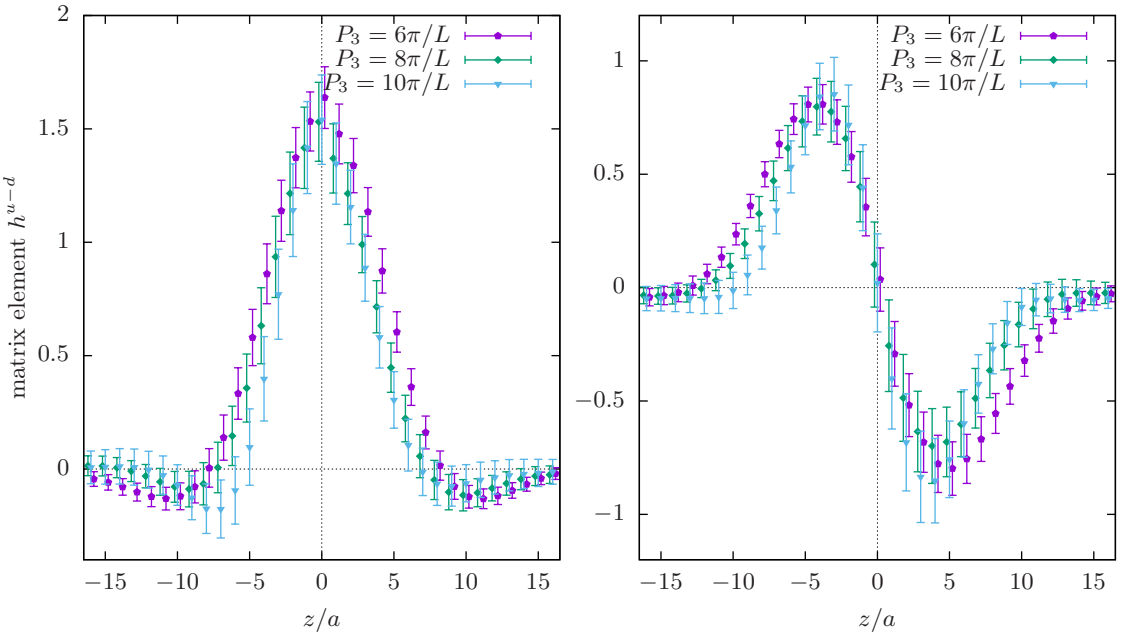

Figure 6: Matrix elements $h^{u-d}(P_3, z)$ (unpolarized operator) for momentum $P_3 = 6\pi/L, 8\pi/L$, and $10\pi/L$, using momentum smearing.

3.3.1 Gaussian smearing

With these chosen parameters, we show in Fig. 9 the results for the quasi distributions, $\tilde{q}(x)$, the distributions before mass corrections, $q(x)$, and the distributions after mass corrections, $q^{(0)}$, for $P_3 = 4\pi/L$, and $6\pi/L$, for both the unpolarized and helicity iso-vector quark distributions, with Gaussian smearing. The phenomenological parameterizations for the experimental data are taken from MSTW [49], CJ12 [50], and ABM11 [51], for the unpolarized case; for the helicity distributions, the parameterizations are taken from DSSV08 [52] and JAM15 [53]. In both cases, we observe a tendency of the calculated distributions to move towards the parameterizations as the nucleon momentum increases, as expected. Also, it is clear from the plots that both the matching and the TMCs become less relevant as the momentum increases, a key observation for the analysis of the data for momentum $8\pi/L$ and $10\pi/L$, as will be done in this section. Our results are compatible with those of Ref. [25]. In particular, we also predict[2] that $\Delta\overline{u}(x) - \Delta\overline{d}(x) > 0$, and such asymmetry also seems to be experimentally observed by the STAR [55] and PHENIX collaborations [56].

Having confirmed our former results for the unpolarized distributions using 6 times more measurements than before, and also having calculated the helicity distributions for the first time in our framework, we are ready to test the feasibility of extending such calculations for higher values of the nucleon momentum. Our results indicate that

[2]The work of Schreiber, Signal, and Thomas [54] was the first one to predict, in the context of a bag model calculation, that $\Delta\overline{u}(x) - \Delta\overline{d}(x) > 0$.

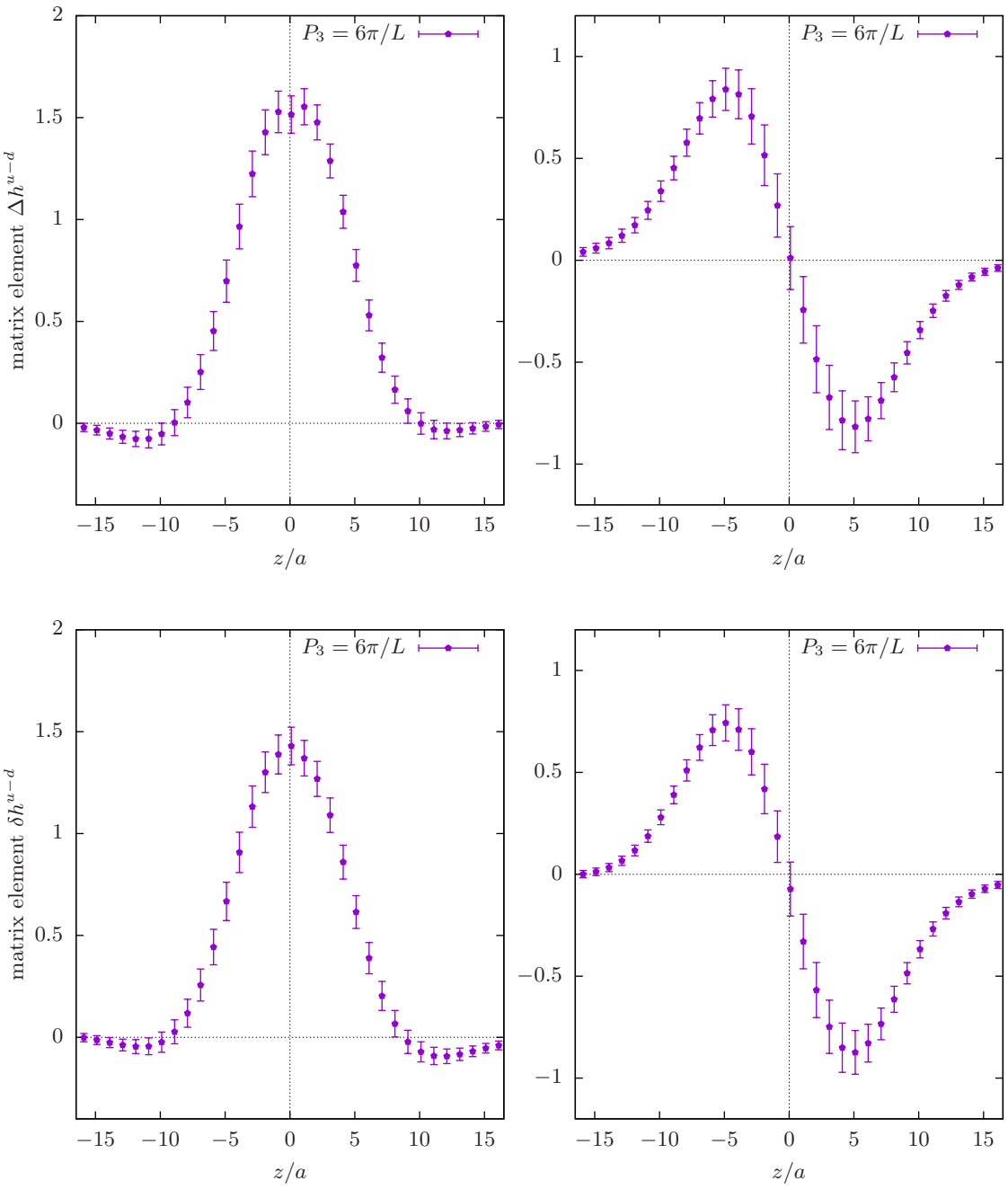

Figure 7: Matrix elements for the helicity and transversity operators for momentum $P_3 = 6\pi/L$, using momentum smearing for the quark fields.

the use of larger values for the momentum improves the agreement between the lattice calculation and the parameterizations, and now this can be reliably tested.

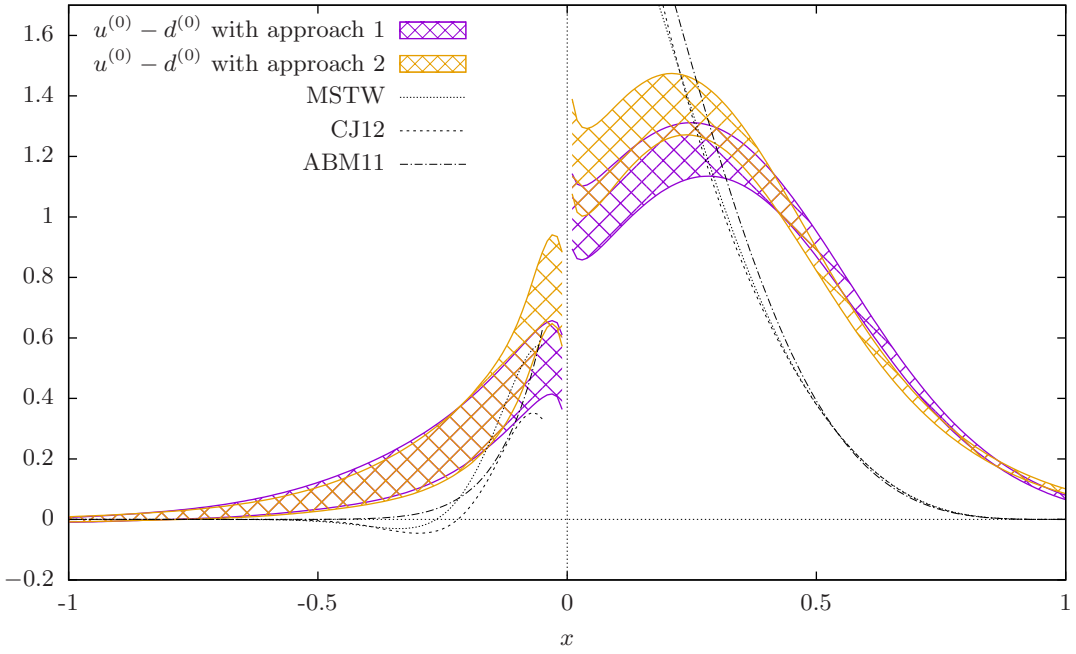

Figure 8: Iso-vector quark distributions calculated with different prescriptions for the TMCs, for $P_3 = 6\pi/L$, using momentum smearing. Prescription (1) is the one of Ref. [26], while prescription (2) is the one of Ref. [25].

3.3.2 Momentum smearing

For the case of momentum smearing, we first recalculate the quasi distributions and the distributions for $P_3 = 6\pi/L$, in order to show that the new results are compatible with those calculated with Gaussian smearing in Fig. 9. The resulting curves, after applying the matching and the TMCs, are shown in Fig. 10, where we also present our results for the transversity distributions. We do not show the parameterizations for the transversity distributions, because they are largely unconstrained (see, for instance, Fig. 3 of Ref. [57]). Future JLab data [58], however, will help to constrain the shape of $\delta u(x)$ and $\delta d(x)$, and precise lattice data can be a valuable guidance in that quest.

We are now ready to show our outcome for $P_3 = 8\pi/L$ and $10\pi/L$, and that is done in Fig. 11. It is clear from this figure that the matching, and the TMCs, provide almost no corrections to the quasi distributions as the nucleon momentum grows, meaning that for $P_3 = 10\pi/L$, the quasi distributions are, essentially, the distributions themselves. This is true mainly in the intermediate and large x regions, the regions where the computation of the quasi distributions in the lattice is valid: we know, from the uncertainty principle relations, that $x_{min} \sim \Lambda_{QCD}/P_3$ is the smallest value for x where quasi distributions can be reliably computed. Moreover, from the data, we also see that the change in the resulting distributions with the nucleon momentum is becoming smaller as P_3 increases. We exemplify this by showing in Fig. 12 the resulting quark distributions for $P_3 = 6\pi/L, 8\pi/L$ and $10\pi/L$, in one plot. Figures 11 and 12 encapsulate the impor-

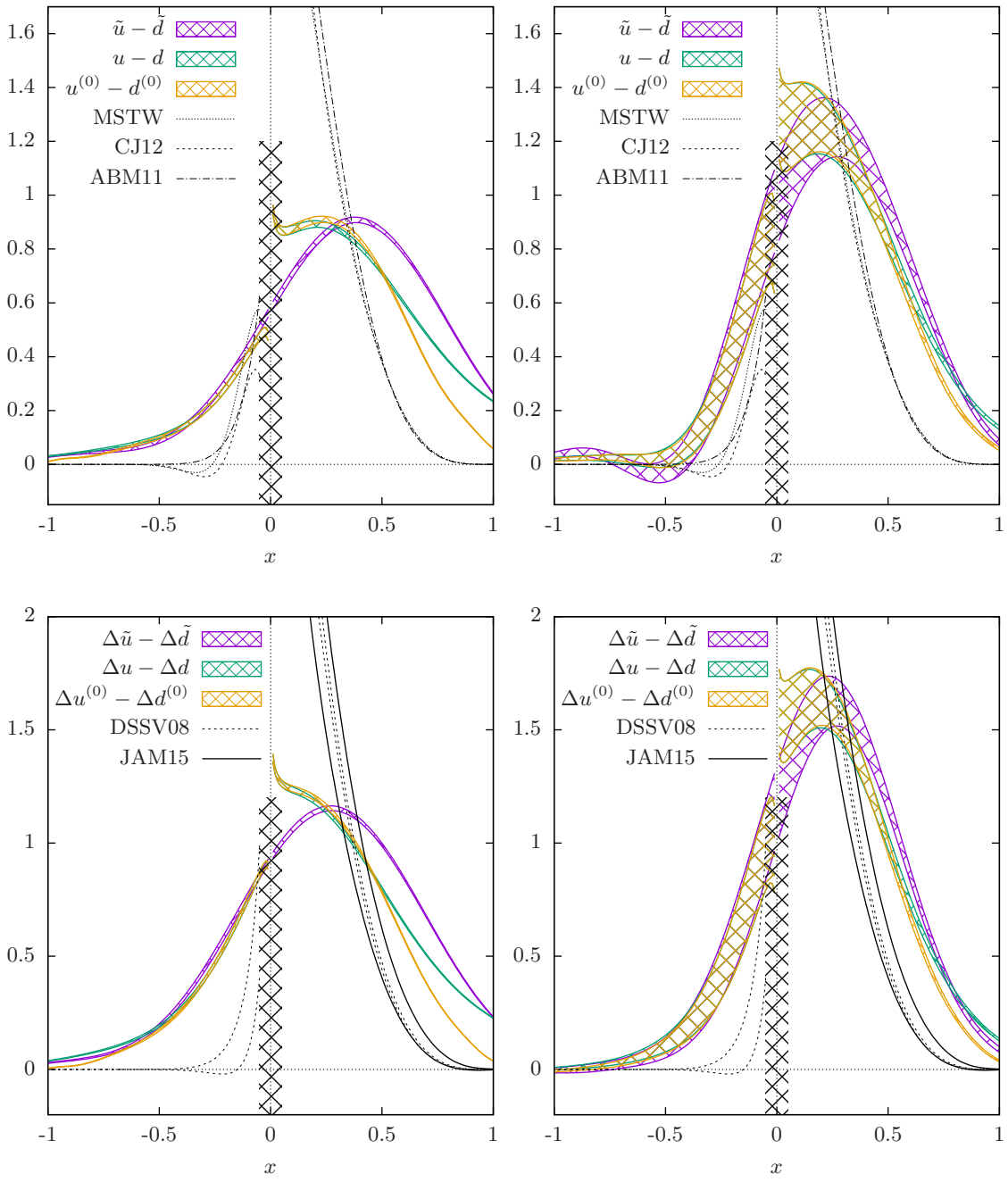

Figure 9: The quark quasi distributions ($\tilde{q}$), the quark distributions (q), and the quark distributions after TMCs are applied ($q^{(0)}$), for the unpolarized and helicity iso-vector combinations, and for $P_3 = 4\pi/L$ (left) and $6\pi/L$ (right). The standard Gaussian smearing for the quark fields is used.

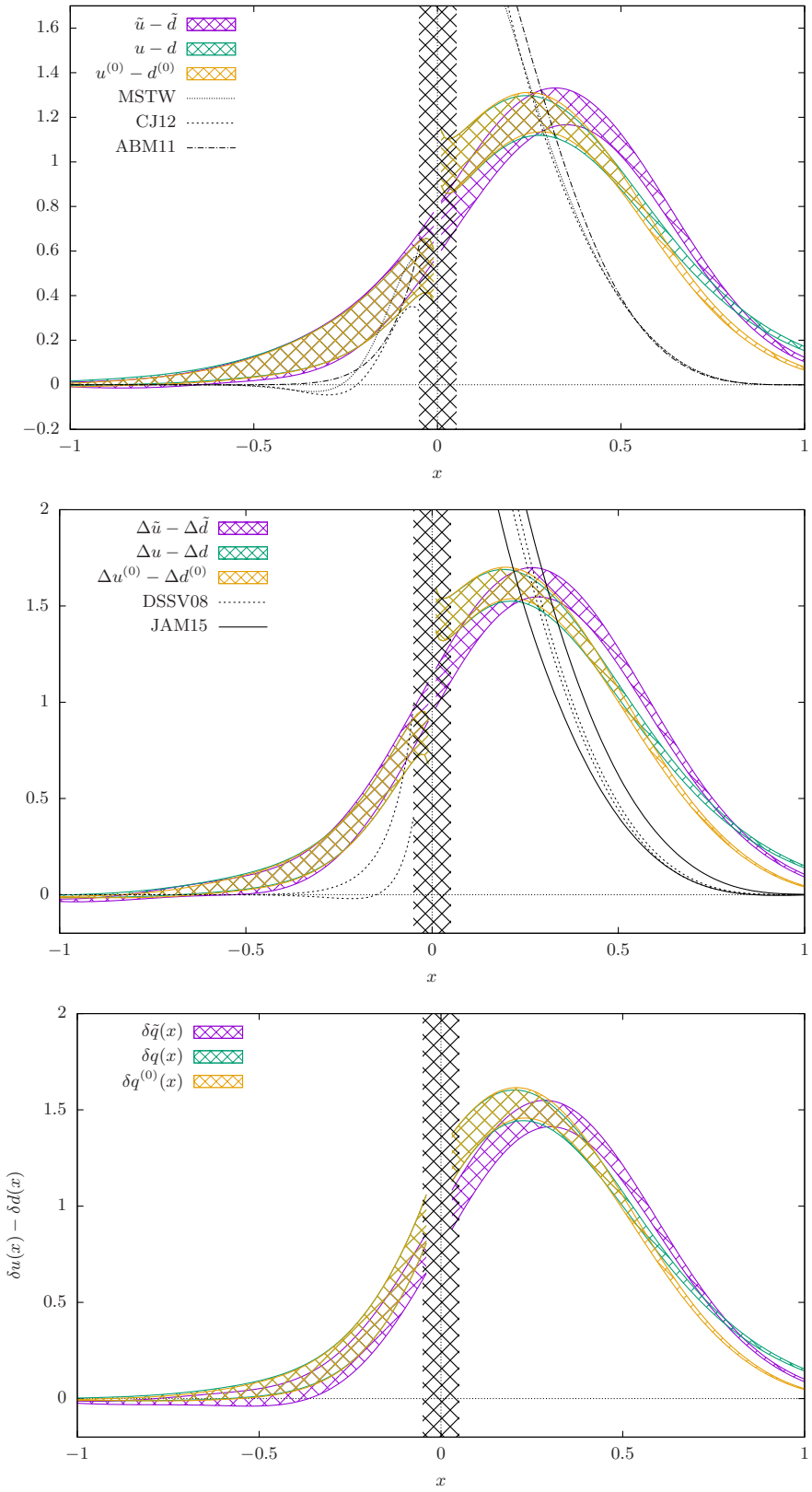

Figure 10: The quark quasi distributions ($\tilde{q}$), the quark distributions (q), and the quark distributions after TMCs are applied ($q^{(0)}$), for the unpolarized, the helicity, and the transversity iso-vector combinations, for $P_3 = 6\pi/L$. The new momentum smearing for the quark fields is used.

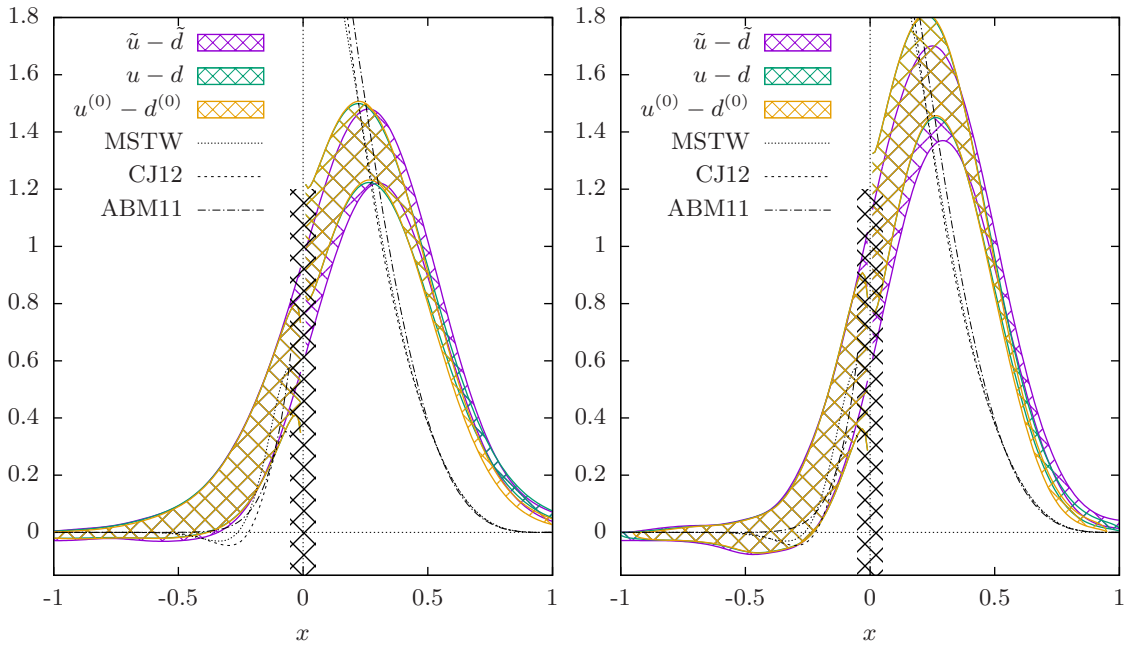

Figure 11: The quark quasi distributions ($\tilde{q}$), the quark distributions (q), and the quark distributions after TMCs are applied ($q^{(0)}$), for the unpolarized iso-vector distributions, and for $P_3 = 8\pi/L$ (left) and $10\pi/L$ (right). Momentum smearing for the quark fields is used.

tant result that we can now compute the quasi-distributions on the lattice for a proton with momentum large enough such that the matching and the mass corrections are significantly smaller than previously possible. Moreover, the resulting distributions have the correct support in x, and are consistent with zero for $x \geq 1$ for the largest proton momentum studied here.

3.4 HYP smearing and renormalization

The natural question to ask at this point is about the influence of renormalization on the results. As we have emphasized above, our matrix elements have not been properly renormalized yet. However, HYP smearing of the Wilson line involved in the computation of the three-point function is expected to bring the values of the renormalization constants of the resulting matrix elements closer to their tree-level values [59]. We demonstrate in this subsection that the effect brought in by HYP smearing leads to an improvement by bringing the extracted PDFs closer to the phenomenological curves.

It is relevant to notice that because the matrix elements are even under the interchange of the positive and the negative z regions and after taking the Hermitian conjugate, as written in Eq. (11), the imaginary part of the matrix elements is odd under the operation $z \to -z$. When performing the Fourier transform, Eq. (5), an asymmetry between the positive and the negative x regions appears exactly because the imaginary part

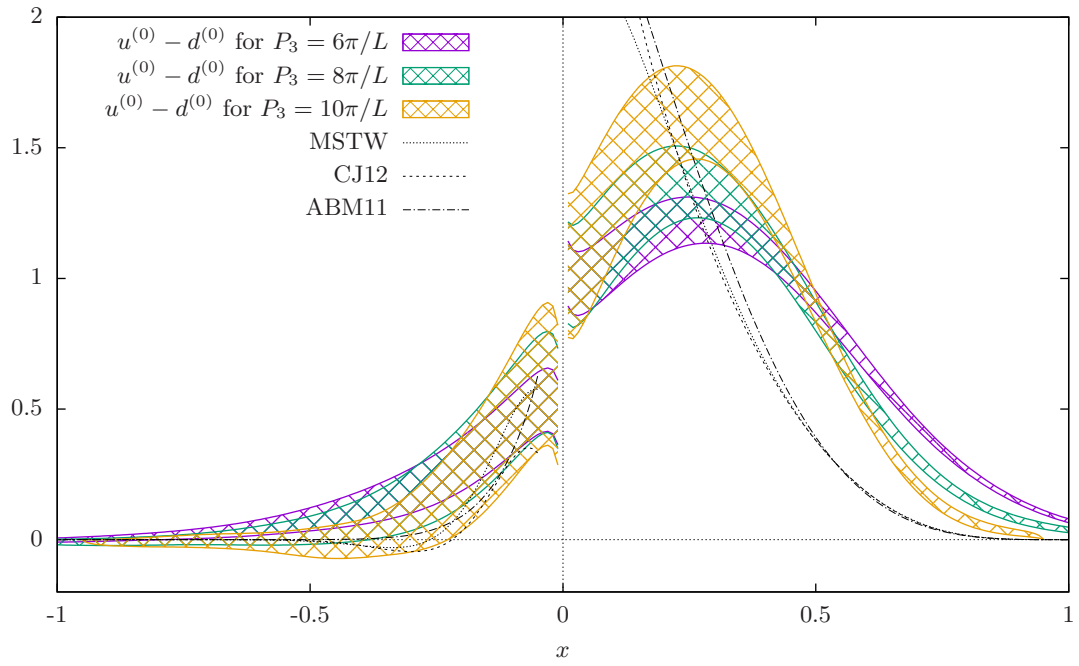

Figure 12: The unpolarized iso-vector quark distributions for momenta $P_3 = 6\pi/L, 8\pi/L$ and $10\pi/L$.

is an odd function. The size of the resulting asymmetry is dependent on how large the imaginary part of the matrix elements is. Moreover, as shown in [26], using smaller values for the nucleon momentum, a sizable imaginary part only appears after HYP smearing is applied, suggesting that renormalization of the inserted operator is fundamental to produce a difference between the positive and the negative x regions. This conclusion is corroborated by Fig. 13, where we compare the unpolarized iso-vector quark distributions for the case where no HYP smearing in the gluon fields is applied and when 5 steps of HYP smearing are used. Without HYP smearing, there is only a very small asymmetry between the positive and the negative x regions, even if the momentum used for the computation is $P_3 = 10\pi/L$. Finally, because quarks in the negative x region correspond to antiquarks in the positive x region, $\overline{q}(x) = -q(-x)$ for the unpolarized case, $\Delta\overline{q}(x) = \Delta q(-x)$ for the helicity case, and $\delta\overline{q}(x) = -\delta q(-x)$ for the transversity case, the asymmetry between quarks and antiquarks in the nucleon, using lattice QCD, is a direct consequence of the relations (11).

As a final note on this subject, we stress that the effect of HYP smearing on the distributions suggests that the properly renormalized results will be closer to the physical PDFs, as compared to the unrenormalized PDFs. However, it is important to point out that the missing renormalization is not the only reason why the phenomenological curves are not reproduced at this stage. In addition to renormalization, there are other lattice effects that need to be controlled, such as cut-off effects and pion mass effects. We provide some evidence for the importance of the latter in the next subsection.

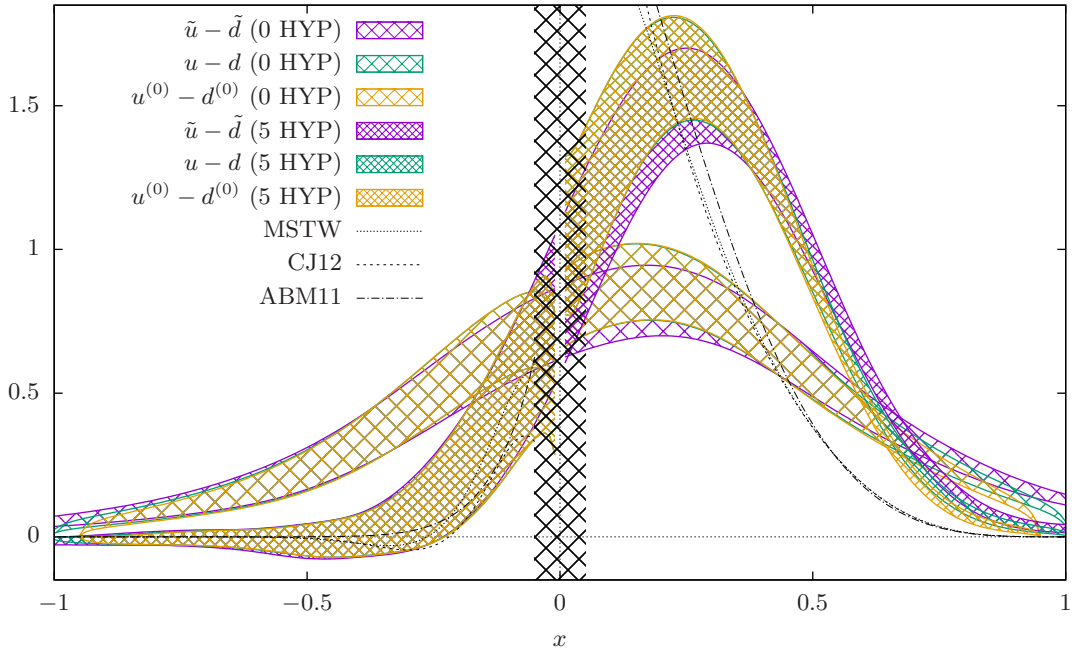

Figure 13: The unpolarized iso-vector quark distributions for momenta $P_3 = 10\pi/L$, with no HYP smearing in the gauge links (thinly filled curves) and with 5 steps of HYP smearing applied (thickly filled curves). Momentum smearing for the quark fields was used. The comparison of 0 and 5 HYP smearing steps shows the importance of renormalization in producing an asymmetry between the x and $-x$ regions, i.e. between quarks and antiquarks.

3.5 Moments of quark distributions

We have also computed the moments of the quark distributions, i.e. quantities that were accessible to earlier lattice investigations, where they are extracted from matrix elements of local currents, e.g. from the forward matrix element of the one-derivative vector current for the first moment of the unpolarized PDF (see Refs. [1, 2, 3, 4, 5] for recent reviews).

We define the n-th moment in the following way. For the unpolarized case,

$$\langle x^n \rangle_q = \int_{-1}^{1} dx\, x^n q(x), \tag{14}$$

where $q(x)$ is the unpolarized iso-vector quark distribution considered in this work. Similar expressions hold for the helicity and transversity distributions. The 0-th moment should be equal to 1 for the unpolarized case. For the helicity case, it should equal the iso-vector axial charge g_A^{u-d}, and for the transversity case the iso-vector tensor charge g_T^{u-d}. We also consider the decomposition of the moments into quark and antiquark parts, i.e. the splitting into the integral over negative (antiquarks) and positive (quarks) values of x in the above formula. For the antiquarks, it corresponds to the following

PDF type	P_3	Smear	Normalization			$\langle x \rangle_q$	$\langle x^2 \rangle_q$
			antiquarks	quarks	total		
unpolarized	3	Gauss	0.187(55)	0.752(56)	0.94(11)	0.219(28)	0.134(12)
		mom	0.145(55)	0.750(53)	0.90(11)	0.240(32)	0.147(15)
	4	mom	0.130(77)	0.743(78)	0.87(15)	0.224(43)	0.116(20)
	5	mom	0.100(88)	0.798(98)	0.90(10)	0.234(46)	0.100(19)
helicity	3	Gauss	0.253(62)	0.920(58)	1.17(12)	0.249(29)	0.154(12)
		mom	0.184(47)	0.931(44)	1.11(9)	0.281(26)	0.154(11)
transversity	3	Gauss	0.175(99)	0.923(95)	1.10(19)	0.309(67)	0.163(35)
		mom	0.169(47)	0.878(44)	1.05(9)	0.276(26)	0.152(11)

Table 1: Moments of the computed PDFs. We show the PDF type, the value of P_3 (in units of $2\pi/L$), the smearing type used (Gauss=Gaussian, mom=momentum), the normalization (zeroth moment) decomposed to give contributions from quarks and antiquarks, the first moment and the second moment. The normalization of helicity and transversity PDFs can be compared to the values of, respectively, $g_A^{u-d} = 1.17(2)$ and $g_T^{u-d} = 1.08(3)$ obtained by the ETMC for the same ensemble of gauge field configurations in Refs. [45, 7]. The first moment values obtained in the same references are: $\langle x \rangle_q = 0.233(9)$ (unpolarized), $\langle x \rangle_{\Delta q} = 0.298(8)$ (helicity) and $\langle x \rangle_{\delta q} = 0.316(12)$ (transversity).

integrals over positive x,

$$\langle x^n \rangle_{\bar{q}} = \int_0^1 dx\, x^n \left(\bar{d}(x) - \bar{u}(x) \right), \tag{15}$$

$$\langle x^n \rangle_{\Delta\bar{q}} = \int_0^1 dx\, x^n \left(\Delta\bar{u}(x) - \Delta\bar{d}(x) \right), \tag{16}$$

$$\langle x^n \rangle_{\delta\bar{q}} = \int_0^1 dx\, x^n \left(\delta\bar{d}(x) - \delta\bar{u}(x) \right), \tag{17}$$

for the unpolarized, helicity and transversity cases, respectively, and where we have used the crossing relations introduced previously in Sec. 3.4 [19].

Our results, obtained from PDFs computed with 5 HYP smearing steps, are shown in Tab. 1. With this computation, we further test the hypothesis that HYP smearing can serve as a crude substitute for renormalization (although not replace it). If such extracted moments agree with the renormalized moments extracted directly, as it will turn out to be, such a hypothesis is further validated.

We find that the normalization condition (total $\langle x^0 \rangle = 1$) is always satisfied (within errors) for the unpolarized case. It is also worth noticing that the integral of the antiquark asymmetry is also compatible with the experimental results (see [19] for a compilation of the experimental and phenomenological results for the light quark sea asymmetry). For example, the New Muon Collaboration [60] finds that $\int_0^1 x^n \left(\bar{d}(x) - \bar{u}(x) \right) = 0.148(39)$.

However, obviously, one can not have a final conclusion based on these numbers, since the PDFs obtained in this work are not rigorously renormalized and the pion mass is non-physical. For the normalization of the helicity and transversity PDFs, we find agreement with ETMC results for the same ensemble of gauge field configurations [45] (with an update in Ref. [7]), $g_A^{u-d} = 1.17(2)$ and $g_T^{u-d} = 1.08(3)$ (at source-sink separation of $16a$).

As for the first moment, the results from ETMC's direct extraction are: $\langle x \rangle_q = 0.233(9)$ (unpolarized), $\langle x \rangle_{\Delta q} = 0.298(8)$ (helicity) and $\langle x \rangle_{\delta q} = 0.316(12)$ (transversity). These values are in a rather good agreement with the ones extracted here, even if they were obtained using a completely different approach. Of course, the point of this comparison is not the expectation that the values will precisely coincide, but rather the qualitative feature that working at this non-physical pion mass, approx. 370 MeV, the quark momentum fraction is significantly above the phenomenological value, around 0.16/0.20 for the unpolarized/helicity case. Conversely, ETMC computations at the physical pion mass lead to the values: $\langle x \rangle_q = 0.208(24)$, $\langle x \rangle_{\Delta q} = 0.229(30)$ and $\langle x \rangle_{\delta q} = 0.306(29)$ [7], i.e. much closer to the phenomenological values (for cases where they are precisely known). This strengthens our expectation that working at the physical pion mass, the PDFs determined from the quasi-PDF approach should also be much closer to the phenomenological curves, i.e. it hints that the pion mass (in addition to the missing renormalization) is to a large extent responsible for the current shape of the extracted PDFs. Nevertheless, other systematic effects, in particular cut-off effects may also play their role.

We also show values for the second moment, $\langle x^2 \rangle_q$. The point of this calculation is to demonstrate that higher moments are obtained with a similar relative precision as the first moments, since their uncertainty depends only on the relative error in the extracted PDFs. This is in opposition to the situation in direct moments extraction in the traditional lattice approach, where higher moments become notoriously difficult beyond the second or third moment and even those can be obtained with a much worse precision, due to a decreasing signal-to-noise ratio and complicated mixing patterns under renormalization.

4 Conclusions and outlook

In this paper, we have provided a calculation of bare parton distribution functions using lattice QCD techniques. In particular, we analyzed the unpolarized, the helicity and the transversity PDFs. In the cases of the unpolarized and helicity PDFs, we have found a good qualitative agreement with the phenomenologically extracted PDFs. In case of the transversity PDF, the uncertainties from the phenomenological analyses are rather high such that the lattice calculations –after a suitable renormalization– have the potential to provide eventually the first theoretical prediction which is, moreover, based only on QCD. As a general observation, the results of our ab initio, non-perturbative lattice calculations show an asymmetry between the quark and the anti-quark distributions, which is a highly non-trivial outcome.

Employing the high statistics analysis in the case of the Gaussian smearing allowed us to reduce the errors for the calculated matrix elements for $P_3 = 4\pi/L$ and $6\pi/L$ by a factor of 2.5 as compared to our previous work [26]. This, in turn, leads to a much better controlled matching to the physical PDFs, which is, however, limited to a maximum momentum of $6\pi/L$. A very promising new direction, to circumvent the problem of having access to only low values of the nucleon momentum, is the use of momentum smearing [29]. We have tested this new smearing technique and found large, $\mathcal{O}(10-100)$, factors of improvement in the signal-to-noise ratio for our matrix elements, and could thus perform the computation of the distributions for a momentum as large as $10\pi/L$. This is an enormous step forward for the computation of PDFs directly in lattice QCD, and Figs. 11 and 12 are our main results in this respect. The resulting quark distributions at these large values of momentum show the correct support in x and, additionally, that their dependence on P_3 starts to become weaker.

Although we only tested the momentum smearing technique on a small number of gluon field configurations, and did not use the full statistics available, we are progressing to use this technique on our ensembles at the physical value of the pion mass [7, 61], employing there the full available statistics. Thanks to this new technique, we have now the prospect to obtain accurate results for high momenta and thus a well controlled matching to the physical PDFs.

Given the results of Fig. 11, the remaining difference to the phenomenologically extracted PDFs is, most probably, due to the large pion mass and to the missing renormalization of the lattice PDFs. The suspicion related to the renormalization is corroborated by comparing results of non-smeared and HYP smeared lattice PDFs – we observe that the HYP smeared PDFs are much closer to the phenomenological ones. However, it is also clear that a significant part of the difference between our result and the phenomenologically extracted PDFs is due to the non-physical pion mass. Computations of hadron structure observables from ensembles at the physical point eliminated a large part of discrepancies with respect to the experimental values. Such discrepancies were typically found in earlier studies that used larger than physical pion masses [1, 7, 8, 9, 10, 11, 12, 13, 14]. In particular, this concerns the first moment of the unpolarized iso-vector PDF, $\langle x \rangle_{u-d}$, for which values in the ballpark between 0.2 and 0.3 were obtained at non-physical pion masses, while studies at the physical point resulted in values close to the experimental one. Hence, the plausible effect of decreasing the pion mass is to shift the curves like the ones in Fig. 12 to the left (in the large-x region), as this decreases $\langle x \rangle_{u-d}$ obtained upon integration of these curves. In the end, we expect that the computation at the physical pion mass, together with renormalization and using large momenta, accessible with the momentum smearing technique, will bring the lattice PDFs very close to the phenomenological ones. We would like to note that since the submission of this work substantial progress has been made on the renormalization of the quasi-PDFs. The authors of Ref. [32] revealed a finite mixing pattern in lattice regularization for certain Dirac structures [32], which led to the development of a complete non-perturbative prescription [33], which was followed closely by [62]. Nevertheless, all other possible systematic effects, like cut-off effects, will also need to be addressed for the ultimate comparison with phenomenology.

Acknowledgments

We thank our fellow members of ETMC for their constant collaboration. In particular helpful discussions with G.C. Rossi are gratefully acknowledged. We are grateful to the John von Neumann Institute for Computing (NIC), the Jülich Supercomputing Center and the DESY Zeuthen Computing Center for their computing resources and support. This work has been supported by the Cyprus Research Promotion Foundation through the Project Cy-Tera (NEA ΥΠΟΔΟΜΗ/ΣΤΡΑΤΗ/0308/31) co-financed by the European Regional Development Fund. K.C. was supported in part by the Deutsche Forschungsgemeinschaft (DFG), project nr. CI 236/1-1. FS was partly supported by CNPq contract number 249168/2013-8. This work has received funding from the European Union's Horizon 2020 research and innovation programme under the Marie Sklodowska-Curie grant agreement No 642069 (HPC-LEAP).

References

[1] M. Constantinou, "Hadron Structure," PoS **LATTICE2014** (2014) 001, arXiv:1411.0078 [hep-lat].

[2] M. Constantinou, "Recent progress in hadron structure from Lattice QCD," PoS **CD15** (2015) 009, arXiv:1511.00214 [hep-lat].

[3] C. Alexandrou and K. Jansen, "Hadron structure from lattice QCD," Nucl. Part. Phys. Proc. **261-262** (2015) 202–217.

[4] C. Alexandrou, "Selected results on hadron structure using state-of-the-art lattice qcd simulations," in Proceedings, 45th International Symposium on Multiparticle Dynamics (ISMD 2015): Kreuth, Germany, October 4-9, 2015. 2015. arXiv:1512.03924 [hep-lat].

[5] S. Syritsyn, "Review of Hadron Structure Calculations on a Lattice," PoS **LATTICE2013** (2014) 009, arXiv:1403.4686 [hep-lat].

[6] H.-W. Lin and H. B. Meyer, eds., Lattice QCD for Nuclear Physics, vol. 889 of Lecture Notes in Physics. Springer, 2015. http://link.springer.com/book/10.1007/978-3-319-08022-2.

[7] A. Abdel-Rehim et al., "Nucleon and pion structure with lattice QCD simulations at physical value of the pion mass," Phys. Rev. **D92** no. 11, (2015) 114513, arXiv:1507.04936 [hep-lat].

[8] G. Bali, S. Collins, M. Göckeler, R. Rödl, A. Schäfer, and A. Sternbeck, "Nucleon generalized form factors from lattice QCD with nearly physical quark masses," PoS **LATTICE2015** (2016) 118, arXiv:1601.04818 [hep-lat].

[9] **PNDME** Collaboration, T. Bhattacharya, V. Cirigliano, S. Cohen, R. Gupta, A. Joseph, H.-W. Lin, and B. Yoon, "Iso-vector and Iso-scalar Tensor Charges of the Nucleon from Lattice QCD," Phys. Rev. **D92** no. 9, (2015) 094511, arXiv:1506.06411 [hep-lat].

[10] S. Durr et al., "Lattice computation of the nucleon scalar quark contents at the physical point," Phys. Rev. Lett. **116** no. 17, (2016) 172001, arXiv:1510.08013 [hep-lat].

[11] **RBC, UKQCD** Collaboration, S. Ohta, "Systematics analyses on nucleon isovector observables in 2+1-flavor dynamical domain-wall lattice QCD near physical mass," PoS **LATTICE2014** (2014) 149, arXiv:1410.8353 [hep-lat].

[12] J. R. Green, J. W. Negele, A. V. Pochinsky, S. N. Syritsyn, M. Engelhardt, and S. Krieg, "Nucleon electromagnetic form factors from lattice QCD using a nearly physical pion mass," Phys. Rev. **D90** (2014) 074507, arXiv:1404.4029 [hep-lat].

[13] J. R. Green, M. Engelhardt, S. Krieg, J. W. Negele, A. V. Pochinsky, and S. N. Syritsyn, "Nucleon Structure from Lattice QCD Using a Nearly Physical Pion Mass," Phys. Lett. **B734** (2014) 290–295, arXiv:1209.1687 [hep-lat].

[14] H.-W. Lin, "Recent progress on nucleon structure with lattice QCD," Int. J. Mod. Phys. Conf. Ser. **25** (2014) 1460039.

[15] C. Alexandrou, M. Constantinou, V. Drach, K. Hadjiyiannakou, K. Jansen, et al., "Evaluation of disconnected quark loops for hadron structure using GPUs," Comput.Phys.Commun. **185** (2014) 1370–1382, arXiv:1309.2256 [hep-lat].

[16] A. Abdel-Rehim, C. Alexandrou, M. Constantinou, V. Drach, K. Hadjiyiannakou, et al., "Disconnected quark loop contributions to nucleon observables in lattice QCD," Phys.Rev. **D89** no. 3, (2014) 034501, arXiv:1310.6339 [hep-lat].

[17] A. J. Chambers et al., "Disconnected contributions to the spin of the nucleon," Phys. Rev. **D92** no. 11, (2015) 114517, arXiv:1508.06856 [hep-lat].

[18] T. Bhattacharya, V. Cirigliano, R. Gupta, H.-W. Lin, and B. Yoon, "Neutron Electric Dipole Moment and Tensor Charges from Lattice QCD," Phys. Rev. Lett. **115** no. 21, (2015) 212002, arXiv:1506.04196 [hep-lat].

[19] W.-C. Chang and J.-C. Peng, "Flavor Structure of the Nucleon Sea," Prog. Part. Nucl. Phys. **79** (2014) 95–135, arXiv:1406.1260 [hep-ph].

[20] A. W. Thomas, "A Limit on the Pionic Component of the Nucleon Through SU(3) Flavor Breaking in the Sea," Phys. Lett. **B126** (1983) 97–100.

[21] A. W. Thomas, W. Melnitchouk, and F. M. Steffens, "Dynamical symmetry breaking in the sea of the nucleon," Phys. Rev. Lett. **85** (2000) 2892–2894, arXiv:hep-ph/0005043 [hep-ph].

[22] X. Ji, "Parton Physics on a Euclidean Lattice," Phys.Rev.Lett. **110** (2013) 262002, arXiv:1305.1539 [hep-ph].

[23] X. Ji, "Parton Physics from Large-Momentum Effective Field Theory," Sci. China Phys. Mech. Astron. **57** (2014) 1407–1412, arXiv:1404.6680 [hep-ph].

[24] H.-W. Lin, J.-W. Chen, S. D. Cohen, and X. Ji, "Flavor Structure of the Nucleon Sea from Lattice QCD," Phys. Rev. **D91** (2015) 054510, arXiv:1402.1462 [hep-ph].

[25] J.-W. Chen, S. D. Cohen, X. Ji, H.-W. Lin, and J.-H. Zhang, "Nucleon Helicity and Transversity Parton Distributions from Lattice QCD," Nucl. Phys. **B911** (2016) 246–273, arXiv:1603.06664 [hep-ph].

[26] C. Alexandrou, K. Cichy, V. Drach, E. Garcia-Ramos, K. Hadjiyiannakou, K. Jansen, F. Steffens, and C. Wiese, "Lattice calculation of parton distributions," Phys. Rev. **D92** no. 1, (2015) 014502, arXiv:1504.07455 [hep-lat].

[27] L. Gamberg, Z.-B. Kang, I. Vitev, and H. Xing, "Quasi-parton distribution functions: a study in the diquark spectator model," Phys. Lett. **B743** (2015) 112–120, arXiv:1412.3401 [hep-ph].

[28] J.-W. Chen, X. Ji, and J.-H. Zhang, "Improved quasi parton distribution through Wilson line renormalization," arXiv:1609.08102 [hep-ph].

[29] G. S. Bali, B. Lang, B. U. Musch, and A. Schäfer, "Novel quark smearing for hadrons with high momenta in lattice QCD," Phys. Rev. **D93** no. 9, (2016) 094515, arXiv:1602.05525 [hep-lat].

[30] X. Ji and J.-H. Zhang, "Renormalization of quasiparton distribution," Phys. Rev. **D92** (2015) 034006, arXiv:1505.07699 [hep-ph].

[31] T. Ishikawa, Y.-Q. Ma, J.-W. Qiu, and S. Yoshida, "Practical quasi parton distribution functions," arXiv:1609.02018 [hep-lat].

[32] M. Constantinou and H. Panagopoulos, "Perturbative Renormalization of quasi-PDFs," arXiv:1705.11193 [hep-lat].

[33] C. Alexandrou, K. Cichy, M. Constantinou, K. Hadjiyiannakou, K. Jansen, H. Panagopoulos, and F. Steffens, "A complete non-perturbative renormalization prescription for quasi-PDFs," arXiv:1706.00265 [hep-lat].

[34] R. P. Feynman, Photon-Hadron Interactions. Frontiers in Physics. Benjamin, Reading, MA, 1972. https://cds.cern.ch/record/102074.

[35] R. L. Jaffe, "Deep inelastic scattering with application to nuclear targets," in Proceedings, Research Program at CEBAF I. 1985. http://alice.cern.ch/format/showfull?sysnb=0073090.

[36] X. Xiong, X. Ji, J.-H. Zhang, and Y. Zhao, "One-loop matching for parton distributions: Nonsinglet case," Phys.Rev. **D90** no. 1, (2014) 014051, arXiv:1310.7471 [hep-ph].

[37] C. Alexandrou, S. Gusken, F. Jegerlehner, K. Schilling, and R. Sommer, "The Static approximation of heavy - light quark systems: A Systematic lattice study," Nucl. Phys. **B414** (1994) 815–855, arXiv:hep-lat/9211042 [hep-lat].

[38] S. Gusken, "A Study of smearing techniques for hadron correlation functions," Nucl. Phys. Proc. Suppl. **17** (1990) 361–364.

[39] C. Alexandrou, K. Cichy, K. Hadjiyiannakou, K. Jansen, F. Steffens, and C. Wiese, "A lattice calculation of parton distributions," in Proceedings, 24th International Workshop on Deep-Inelastic Scattering and Related Subjects (DIS 2016): Hamburg, Germany, April 11-25, 2016. 2016. arXiv:1609.00172 [hep-lat].

[40] G. Martinelli and C. T. Sachrajda, "A Lattice Study of Nucleon Structure," Nucl. Phys. **B316** (1989) 355.

[41] **ETM** Collaboration, C. Alexandrou et al., "A Stochastic Method for Computing Hadronic Matrix Elements," Eur.Phys.J. **C74** no. 1, (2014) 2692, arXiv:1302.2608 [hep-lat].

[42] C. Alexandrou, K. Cichy, V. Drach, E. Garcia-Ramos, K. Hadjiyiannakou, et al., "First results with twisted mass fermions towards the computation of parton distribution functions on the lattice," PoS **LATTICE2014** (2014) 135, arXiv:1411.0891 [hep-lat].

[43] A. Hasenfratz and F. Knechtli, "Flavor symmetry and the static potential with hypercubic blocking," Phys.Rev. **D64** (2001) 034504, arXiv:hep-lat/0103029 [hep-lat].

[44] **ETM** Collaboration, C. Alexandrou, M. Constantinou, and H. Panagopoulos, "Renormalization functions for Nf=2 and Nf=4 Twisted Mass fermions," arXiv:1509.00213 [hep-lat].

[45] C. Alexandrou, M. Constantinou, S. Dinter, V. Drach, K. Jansen, et al., "Nucleon form factors and moments of generalized parton distributions using $N_f = 2 + 1 + 1$ twisted mass fermions," Phys.Rev. **D88** no. 1, (2013) 014509, arXiv:1303.5979 [hep-lat].

[46] R. Baron, P. Boucaud, J. Carbonell, A. Deuzeman, V. Drach, et al., "Light hadrons from lattice QCD with light (u,d), strange and charm dynamical quarks," JHEP **1006** (2010) 111, arXiv:1004.5284 [hep-lat].

[47] **European Twisted Mass** Collaboration, N. Carrasco et al., "Up, down, strange and charm quark masses with $N_f = 2+1+1$ twisted mass lattice QCD," Nucl. Phys. **B887** (2014) 19–68, arXiv:1403.4504 [hep-lat].

[48] D. S. Roberts, W. Kamleh, D. B. Leinweber, M. S. Mahbub, and B. J. Menadue, "Accessing High Momentum States In Lattice QCD," Phys. Rev. **D86** (2012) 074504, arXiv:1206.5891 [hep-lat].

[49] A. Martin, W. Stirling, R. Thorne, and G. Watt, "Parton distributions for the LHC," Eur.Phys.J. **C63** (2009) 189–285, arXiv:0901.0002 [hep-ph].

[50] J. Owens, A. Accardi, and W. Melnitchouk, "Global parton distributions with nuclear and finite-Q^2 corrections," Phys.Rev. **D87** no. 9, (2013) 094012, arXiv:1212.1702 [hep-ph].

[51] S. Alekhin, J. Blümlein, and S. Moch, "Parton Distribution Functions and Benchmark Cross Sections at NNLO," Phys.Rev. **D86** (2012) 054009, arXiv:1202.2281 [hep-ph].

[52] D. de Florian, R. Sassot, M. Stratmann, and W. Vogelsang, "Extraction of Spin-Dependent Parton Densities and Their Uncertainties," Phys. Rev. **D80** (2009) 034030, arXiv:0904.3821 [hep-ph].

[53] **Jefferson Lab Angular Momentum** Collaboration, N. Sato, W. Melnitchouk, S. E. Kuhn, J. J. Ethier, and A. Accardi, "Iterative Monte Carlo analysis of spin-dependent parton distributions," Phys. Rev. **D93** no. 7, (2016) 074005, arXiv:1601.07782 [hep-ph].

[54] A. W. Schreiber, A. I. Signal, and A. W. Thomas, "Structure functions in the bag model," Phys. Rev. **D44** (1991) 2653–2662.

[55] **STAR** Collaboration, L. Adamczyk et al., "Measurement of longitudinal spin asymmetries for weak boson production in polarized proton-proton collisions at RHIC," Phys. Rev. Lett. **113** (2014) 072301, arXiv:1404.6880 [nucl-ex].

[56] **PHENIX** Collaboration, A. Adare et al., "Measurement of parity-violating spin asymmetries in $W^{\pm}$ production at midrapidity in longitudinally polarized p+p collisions," Phys. Rev. **D93** no. 5, (2016) 051103, arXiv:1504.07451 [hep-ex].

[57] Z.-B. Kang, A. Prokudin, P. Sun, and F. Yuan, "Extraction of Quark Transversity Distribution and Collins Fragmentation Functions with QCD Evolution," Phys. Rev. **D93** no. 1, (2016) 014009, arXiv:1505.05589 [hep-ph].

[58] J. Zhang, "JLab E12-10-006 Experiment, Target Single Spin Asymmetry in Semi-Inclusive Deep-Inelastic Electro Pion Production on a Transversely Polarized ^3He Target at 8.8 and 11 GeV," 2016. https://www.jlab.org/exp_prog/proposals/14/E12-10-006A.pdf and https://hallaweb.jlab.org/wiki/index.php/SoLID.

[59] S. Capitani, S. Durr, and C. Hoelbling, "Rationale for UV-filtered clover fermions," JHEP **11** (2006) 028, arXiv:hep-lat/0607006 [hep-lat].

[60] **New Muon** Collaboration, M. Arneodo et al., "A Reevaluation of the Gottfried sum," Phys. Rev. **D50** (1994) R1–R3.

[61] **ETM** Collaboration, A. Abdel-Rehim et al., "Simulating QCD at the Physical Point with $N_f = 2$ Wilson Twisted Mass Fermions at Maximal Twist," arXiv:1507.05068 [hep-lat].

[62] J.-W. Chen, T. Ishikawa, L. Jin, H.-W. Lin, Y.-B. Yang, J.-H. Zhang, and Y. Zhao, "Parton Distribution Function with Non-perturbative Renormalization from Lattice QCD," arXiv:1706.01295 [hep-lat].